Linear refractive index and absorption measurements of nonlinear optical liquids in the visible and near-infrared spectral region

S. Kedenburg, M. Vieweg, T. Gissibl, and H. Giessen*

4th *Physics Institute and Research Center SCOPE, University of Stuttgart, 70550 Stuttgart, Germany*

**h.giessen@pi4.uni-stuttgart.de*

Abstract: Liquid-filled photonic crystal fibers and optofluidic devices require infiltration with a variety of liquids whose linear optical properties are still not well known over a broad spectral range, particularly in the near infrared. Hence, dispersion and absorption properties in the visible and near-infrared wavelength region have been determined for distilled water, heavy water, chloroform, carbon tetrachloride, toluene, ethanol, carbon disulfide, and nitrobenzene at a temperature of 20 °C. For the refractive index measurement a standard Abbe refractometer in combination with a white light laser and a technique to calculate correction terms to compensate for the dispersion of the glass prism has been used. New refractive index data and derived dispersion formulas between a wavelength of 500 nm and 1600 nm are presented in good agreement with sparsely existing reference data in this wavelength range. The absorption coefficient has been deduced from the difference of the losses of several identically prepared liquid filled glass cells or tubes of different lengths. We present absorption data in the wavelength region between 500 nm and 1750 nm.

OCIS codes: (160.4330) Nonlinear optical materials; (260.2030) Dispersion; (300.1030) Absorption.

References and links

1. D. Psaltis, S. R. Quake, and C. Yang, "Developing optofluidic technology through the fusion of microfluidics and optics," Nature (London) **442,** 381–386 (2006).
2. C. Monat, P. Domachuk, and B. J. Eggleton, "Integrated optofluidics: A new river of light," Nat. Photonics **1,** 106–114 (2007).
3. R. Zhang, J. Teipel, and H. Giessen, "Theoretical design of a liquid-core photonic crystal fiber for supercontinuum generation," Opt. Express **14,** 6800–6812 (2006).
4. M. Vieweg, T. Gissibl, S. Pricking, B. T. Kuhlmey, D. C. Wu, B. J. Eggleton, and H. Giessen, "Ultrafast nonlinear optofluidics in selectively liquid-filled photonic crystal fibers," Opt. Express **18,** 25232–25240 (2010).
5. J. Bethge, A. Husakou, F. Mitschke, F. Noack, U. Griebner, G. Steinmeyer, and J. Herrmann, "Two-octave supercontinuum generation in a water-filled photonic crystal fiber," Opt. Express **18,** 6230–6240 (2010).
6. S. Pricking and H. Giessen, "Generalized retarded response of nonlinear media and its influence on soliton dynamics," Opt. Express **19,** 2895–2903 (2011).
7. K. Kieu, L. Schneebeli, R. A. Norwood, and N. Peyghambarian, "Integrated liquid-core optical fibers for ultra-efficient nonlinear liquid photonics," Opt. Express **20,** 8148–8154 (2012).
8. M. Vieweg, S. Pricking, T. Gissibl, Y. V. Kartashov, L. Torner, and H. Giessen, "Tunable ultrafast nonlinear optofluidic coupler," Opt. Lett. **37,** 1058–1060 (2012).

#170502 - $15.00 USD Received 12 Jun 2012; revised 26 Sep 2012; accepted 2 Oct 2012; published 15 Oct 2012

9. S. Pricking, M. Vieweg, and H. Giessen, "Influence of the retarded response on an ultrafast nonlinear optofluidic fiber coupler," Opt. Express **19,** 21673–21679 (2011).
10. K. Kieu, L. Schneebeli, E. Merzlyak, J. M. Hales, A. DeSimone, J. W. Perry, R. A. Norwood, and N. Peyghambarian, "All-optical switching based on inverse Raman scattering in liquid-core optical fibers," Opt. Lett. **37,** 942–944 (2012).
11. M. Vieweg, T. Gissibl, Y. V. Kartashov, L. Torner, and H. Giessen, "Spatial solitons in optofluidic waveguide arrays with focusing ultrafast Kerr nonlinearity," Opt. Lett. **37,** 2454–2456 (2012).
12. W. Gao, D. Sun, Y. F. Bi, J. Y. Li, and Y. L. Wang, "Stimulated Brillouin scattering with high reflectivity and fidelity in liquid-core optical fibers," Appl. Phys. B: Lasers Opt. **107,** 355–359 (2012).
13. M. C. P. Huy, A. Baron, S. Lebrun, R. Frey, and P. Delaye, "Characterization of self-phase modulation in liquid filled hollow core photonic bandgap fibers," J. Opt. Soc. Am. B **27,** 1886–1893 (2010).
14. R. Zhang, J. Teipel, X. Zhang, D. Nau, and H. Giessen, "Group velocity dispersion of tapered fibers immersed in different liquids," Opt. Express **12,** 1700–1707 (2004).
15. A. Samoc, "Dispersion of refractive properties of solvents: Chloroform, toluene, benzene, and carbon disulfide in ultraviolet, visible, and near-infrared," J. Appl. Phys. **94,** 6167–6174 (2003).
16. J. Rheims, J. Köser, and T. Wriedt, "Refractive-index measurements in the near-IR using an Abbe refractometer," Meas. Sci. Technol. **8,** 601–605 (1997).
17. K. C. Kao and T. W. Davies, "Spectrophotometric studies of ultra low loss optical glasses 1: single beam method," J. Phys. E: Sci. Instrum. **1,** 1063–1068 (1968).
18. M. Daimon and A. Masumura, "Measurement of the refractive index of distilled water from the near-infrared region to the ultraviolet region," Appl. Opt. **46,** 3811–3820 (2007).
19. J. Curcio and C. Petty, "The near infrared absorption spectrum of liquid water," J. Opt. Soc. Am. **41,** 302–304 (1951).
20. R. M. Pope and E. S. Fry, "Absorption spectrum (380-700 nm) of pure water: II. Integrating cavity measurements," Appl. Opt. **36,** 8710–8723 (1997).
21. D. N. Nikogosyan, "Chapter 8: Liquids," in *Properties of Optical and Laser-Related Materials: A Handbook,* (John Wiley & Sons, Chichester, 1997), pp. 400–495.
22. M. J. Weber, "Section 5: Liquids," in *Handbook of Optical Materials,* (CRC Press LLC, Boca Raton, 2003), pp. 373–393.
23. Carl Zeiss AG, Correction tables for the Abbe rfractometer model A with serial number 7, Oberkochen, Germany.
24. Carl Zeiss AG, Engineering drawing for the measuring prism 7, Oberkochen, Germany.
25. Schott AG, Refractive index of SF 13, Mainz, Germany.
26. B. Metzger, A. Steinmann, F. Hoos, S. Pricking, and H. Giessen, "Compact laser source for high-power white-light and widely tunable sub 65 fs laser pulses," Opt. Lett. **35,** 3961–3963 (2010).
27. Thorlabs, Bandpass filter, `http://www.thorlabs.de/navigation.cfm?Guide_ID=2210`.

1. Introduction

Liquids offer striking possibilities for the field of optics. New optical devices have been developed which opened a new field: optofluidics, which combines liquids and photonics [1, 2]. This field has encountered an increased amount of interest in the recent past due to novel flexible concepts.

Liquids are especially suited for generating supercontinua due to their relatively high nonlinear refractive index n_2 with respect to solids. Examples for applications are include selectively liquid-filled photonic crystal fibers [3–6], and liquid-core optical fibers [7] whose dispersion properties can be tailored accordingly for the formation of a supercontinuum. Liquid-filled patterns in such fibers allow for the realization of directional couplers [8, 9], all-optical switching [10] as well as discrete optofluidic spatial solitons in waveguide arrays [11]. Furthermore, characteristics of stimulated Brillouin scattering [12] and self-phase modulation [13] can be studied. Also pulse propagation in tapered fibers immersed in liquids can be tailored [14]. Moreover, the transparency in the visible and near-infrared range plays an important role for unobstructed propagation of light in these structures.

There is an increasing need for rapid and easy measurements of linear optical properties of nonlinear liquids over a broad wavelength range. The knowledge of the linear refractive index n and the absorption coefficient α are important to control the optical properties and to determine n_2 [15].

Due to the fact that published papers [15–20] and reference books [21, 22] currently cannot

#170502 - $15.00 USD Received 12 Jun 2012; revised 26 Sep 2012; accepted 2 Oct 2012; published 15 Oct 2012

cover a broad wavelength range in the visible and near-infrared and some data even seem to not exist in published form, we take measurements in regions which have previously not been investigated to our knowledge.

In this paper precise constants for Cauchy and Sellmeier dispersion equations of linear refractive indices at a temperature of 20 °C are derived from measurement data between a wavelength of 500 nm and 1600 nm for the following eight liquids: distilled water (H_2O), heavy water (D_2O), chloroform ($CHCl_3$), carbon tetrachloride (CCl_4), toluene (C_7H_8), ethanol (C_2H_6O), carbon disulfide (CS_2), and nitrobenzene ($C_6H_5NO_2$). A measurement method which is based on an extension of a standard Abbe refractometer is used to determine $n(\lambda)$ [16]. The required correction terms for the application in the near-infrared and the experimental realization are described in detail.

Furthermore, the absorption coefficient α as a function of wavelength is given between 500 nm and 1750 nm for distilled water, heavy water, chloroform, toluene, ethanol, and carbon tetrachloride (up to a wavelength of 1500 nm). For the measurement of α thin glass cells or long tubes filled with the liquids have been used, depending on the magnitude of absorption. Accurate alignments of the samples were required because α has been calculated from the difference of the losses of several equally prepared specimens of different lengths [17]. The description of the utilized methods and the experimental setups are also presented in this paper.

The structure of the paper is as follows: First the measurement techniques and the experimental setups for the determination of the linear refractive index and the absorption coefficients are described. Second, in Section 3, the measurement results are presented, starting with the refractive index values and dispersion curves, followed by the absorption spectra of the investigated liquids. The absorption coefficient values are given in the supplement as comma-separated value text files.

2. Measurement techniques

2.1. Refractive index

2.1.1. **Abbe refractometer**

An easy and precise method to measure the linear refractive index n in the visible spectral range is provided by an Abbe refractometer. Commonly, such instruments are designed for the use at the wavelength of the sodium D line (589.3 nm). Correction tables enable the use of the refractometer in the complete spectral range covered by the listed values therein. A different description is given in the paper of J. Rheims et al. [16] which allows determination of the refractive index over a wider wavelength regime. However, since the refractometer is an optical measurement device which is read out by naked eye, the wavelength region is still limited to the visible. Only by using infrared-cameras as replacement for the human eye, the method can be extended to the infrared-region.

Regardless of the wavelength, the general working principle is based on the dependence of the angle of total reflection from the refractive index of the investigated liquid. The Abbe refractometer is composed of two orthogonal prisms as shown in Fig. 1.

To apply the principle of total reflection the refractive index of the investigated liquid n_{liq} has to be smaller than the refractive index of the measuring prism n_{pr}. The specimen is placed between the two prisms and the incoming light is transmitted only in an angular range below the angle of total reflection α_T, generating a sharp separation line between the bright and the dark range. This image can be observed with the eyepiece of the refractometer. Matching the separation line with the point of intersection of a reticle allows for readout of the measured refractive index n'_{liq} from a scale.

However, the measured refractive index n'_{liq} only corresponds to the actual refractive index

#170502 - $15.00 USD Received 12 Jun 2012; revised 26 Sep 2012; accepted 2 Oct 2012; published 15 Oct 2012

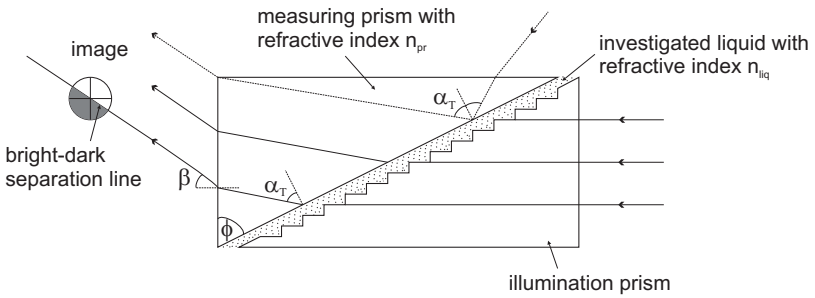

Fig. 1. Beam path in the Abbe refractometer: in transmission mode (solid line) the incoming light passes the illumination prism and is scattered in all directions at the rough surface. However, the light is only transmitted into the measuring prism if the incident angle is below the angle of total reflection α_T. The image displays a sharp separation between the bright and dark range. The image is observed with a telescope and the point of intersection of the reticle has to be adjusted to this separation line. One can then read the measured refractive index n'_{liq} from a scale of the refractometer; in reflection mode (dotted line) the measuring prism is directly illuminated and the incoming light is only reflected in the angular range above the angle of total reflection. Hence, the bright and the dark range are interchanged which does not affect the deflection angle β which has a fixed geometrical relationship to the measured refractive index (see Eq. (5)). ϕ is the prism apex angle which is 63 °in our case.

n_{liq} of the liquid at the sodium D line at $\lambda_D = 589.3$ nm because of the used calibration from the manufacturer Carl Zeiss. To deduce the refractive index n_{liq} also at other wavelengths one has to apply a correction term Δn_{liq} to n'_{liq} to compensate for the dispersion of the glass prism. Correction tables are offered by the manufacturer of the refractometer where Δn_{liq} depends on the illumination wavelength, the measured refractive index, and the used glass prism. However, the correction data are only provided in the visible spectral range between 400 nm and 680 nm [23].

To extend the application range of the refractometer one has to establish a relationship between the deflection angle β and the displayed refractive index n'_{liq} from the scale of the refractometer. This geometrical relationship has to be determined only once because it is not affected by changing the illumination wavelength [16].

2.1.2. **Correction terms**

The refractive index of a liquid is given by Snellius' law as

$$n_{liq} = n_{pr} \sin \alpha_T . \tag{1}$$

By geometrical thoughts and trigonometrical identities (see Fig. 1) and the fact that the change in the refractive index with temperature is negligible for the glass prism [16] one obtains

$$n_{liq}(\lambda, T) = \sin\phi \sqrt{n_{pr}^2(\lambda) - \sin^2\beta(\lambda, T)} - \cos\phi \sin\beta(\lambda, T). \tag{2}$$

Thus, the refractive index of the liquid for a certain wavelength and temperature is a function of the deflection angle β, the refractive index n_{pr}, and the apex angle ϕ of the glass prism.

In order to obtain the actual refractive index of the liquid n_{liq}, the measured refractive index n'_{liq} has to be corrected by the term Δn_{liq}

$$n_{liq}(\lambda, T) = n'_{liq}(\lambda, T) + \Delta n_{liq}(\lambda, n'_{liq}). \tag{3}$$

#170502 - $15.00 USD Received 12 Jun 2012; revised 26 Sep 2012; accepted 2 Oct 2012; published 15 Oct 2012

As the Abbe refractometer is calibrated with respect to the sodium D line, $\Delta n_{liq}(\lambda_D, n'_{liq})$ becomes zero and n_{liq} is equal to n'_{liq} for this wavelength (see Eq. (3)). Replacing n_{liq} by n'_{liq} in Eq. (2) one obtains the desired fixed relationship between n'_{liq} and β

$$n'_{liq}(\lambda_D, T) = \sin\phi \sqrt{n^2_{pr}(\lambda_D) - \sin^2\beta(\lambda_D, T)} - \cos\phi \sin\beta(\lambda_D, T). \tag{4}$$

Solving Eq. (4) for β yields

$$\sin\beta(\lambda, T) = \sin\phi \sqrt{n^2_{pr}(\lambda_D) - n'^2_{liq}(\lambda, T)} - n'_{liq}(\lambda, T)\cos\phi. \tag{5}$$

Hence, by inserting Eq. (5) into Eq. (2) the expression for the actual refractive index reads

$$\begin{aligned} n_{liq}(\lambda, T, n'_{liq}) \quad = \quad & \sin\phi[n^2_{pr}(\lambda) - (\sin\phi \sqrt{n^2_{pr}(\lambda_D) - n'^2_{liq}(\lambda, T)} - \\ & n'_{liq}(\lambda, T)\cos\phi)^2]^{1/2} - \\ & \cos\phi(\sin\phi \sqrt{n^2_{pr}(\lambda_D) - n'^2_{liq}(\lambda, T)} - n'_{liq}(\lambda, T)\cos\phi). \end{aligned} \tag{6}$$

This equation gives the actual refractive index at a certain wavelength in dependence of the prism dispersion, the prism apex angle, and the measured index value n'_{liq}.

In our experiment we use an Abbe refractometer Model A from Carl Zeiss with the serial number 7 and device number 64305. The apex angle of the glass prism ϕ is given in the engineering drawing as 63 ° in the present case [24]. The refractive index of the glass prism made from Schott SF13 glass is given from the glass manufacturer at different wavelengths [25]. At $\lambda_D = 589.3$ nm the refractive index of the prism is $n_{pr}(\lambda_D) = 1.74054$. For $n_{pr}(\lambda)$ the Cauchy formula in Eq. (7) is used:

$$n_{pr} = 1.70708 + \frac{10943.47279}{\lambda^2} + \frac{2.54416 \times 10^8}{\lambda^4} + \frac{3.46802 \times 10^{13}}{\lambda^6} - 2.93242 \times 10^{-9}\lambda^2. \tag{7}$$

The Cauchy formula together with the given refractive indices of SF13 are plotted in Fig. 2.

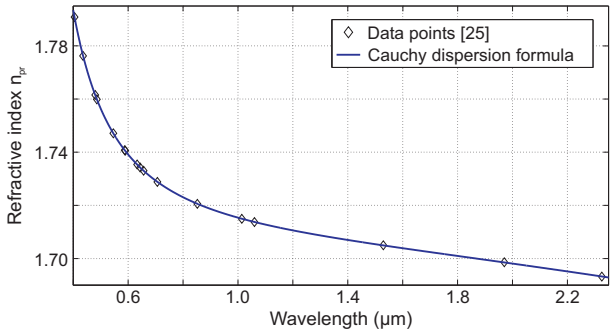

Fig. 2. Dispersion of refractive index of the measuring prism made of SF13. The data points (diamonds) are listed in the datasheet from the glass manufacturer Schott [25]. The calculated Cauchy dispersion formula (blue line) is given in Eq. (7).

For verification the calculated correction term Δn_{liq} is compared with data from a correction table provided by Zeiss at two wavelengths of $\lambda = 500$ nm and $\lambda = 680$ nm [23]. The results are plotted in Fig. 3. Δn_{liq} matches very well with the original data given by Zeiss and the maximum deviation is less than 1×10^{-4} at 500 nm. At a wavelength of 680 nm the deviation

#170502 - $15.00 USD Received 12 Jun 2012; revised 26 Sep 2012; accepted 2 Oct 2012; published 15 Oct 2012

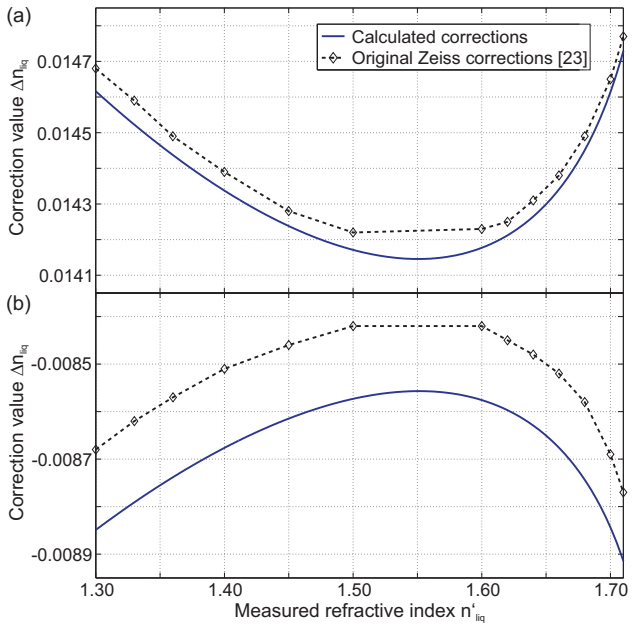

Fig. 3. The calculated correction term Δn_{liq} (blue line) for our Abbe refractometer from Eq. (6) as a function of the measured refractive index n'_{liq} at a wavelength of (a) 500 nm and (b) 680 nm in comparison with original data (dashed line) from a correction table provided by Carl Zeiss AG [23].

is slightly more pronounced but always below 2×10^{-4} which allows the use of the described method for calculating the correction terms in the complete wavelength region of interest.

In Fig. 4 absolute values of the calculated correction terms Δn_{liq} are shown for several wavelengths in the visible and near-infrared range, as used in our experiment. Below the wavelength of 589.3 nm the corrections are positive, above λ_D they are negative.

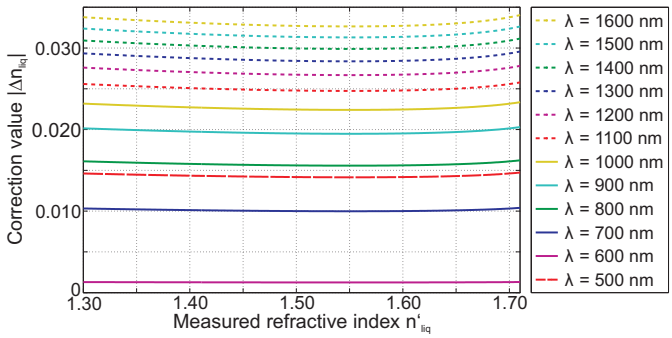

Fig. 4. Absolute values of the calculated correction terms Δn_{liq} for our Abbe refractometer from Eq. (6) as a function of the measured refractive index n'_{liq} for different wavelengths.

2.1.3. **Refractometer setup**

The experimental setup is shown in Fig. 5a. The Abbe refractometer (Carl Zeiss, model A, serial number 7, device number 64305, see Fig. 5b) is connected to a cooling system to ensure

#170502 - $15.00 USD Received 12 Jun 2012; revised 26 Sep 2012; accepted 2 Oct 2012; published 15 Oct 2012

a constant temperature of 20 °C which can be controlled by a thermometer at the illumination prism. Due to the cooling mechanism the temperature varies in the range of ± 0.5 °C. A supercontinuum generated by a tapered fiber with fiber diameters of 2.5 μm or 3.0 μm, respectively, are used as light sources [26]. A modelocked Ti:Sapphire femtosecond laser at a central wavelength of 800 nm for the 2.5 μm fiber and a modelocked PolarOnyx Uranus fiber laser with fs pulse compressor at a central wavelength of 1035 nm for the 3.0 μm fiber serve as pump sources to ensure a broad spectral range. White light spectra are shown in Fig. 6. Bandpass filters with a bandwidth of $\Delta\lambda = 10$ nm and a tolerance of the central filter wavelength of ± 2 nm [27] are placed into the laser beam path to select certain wavelengths between 500 nm and 1600 nm.

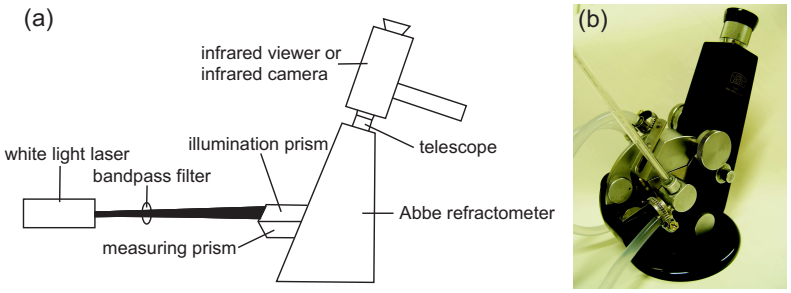

Fig. 5. (a) Experimental setup for refractive index measurements with the Abbe refractometer in the visible and near-infrared in transmission mode. In reflection mode one directly illuminates the measuring prism. (b) Abbe refractometer model A from Carl Zeiss.

Depending on the absorption strength of the investigated liquid, the refractometer can also be used in reflection mode to enhance the visibility of the dark-bright separation line. Therefore a second illumination window is mounted at the front of the measuring prism. Thus the beam path shown in Fig. 1 is somewhat modified which does not affect the formula of the correction term. The compensator of the refractometer, which filters out the sodium D line and deflects other wavelengths, is set during the whole measurement to the position 30 in which no wavelength dependent beam deviation occurs. To match the reticle with the separation line an infrared viewer of FJW Optical Systems (Find-R-Scope Model 84499A) is used in the wavelength range between 500 nm and 1200 nm. Due to the reduced sensitivity of the infrared viewer above a wavelength of 1200 nm, an infrared camera NIR-300FGE from Allied Vision Technologies is used in the wavelength region between 900 nm and 1600 nm.

2.2. Absorption coefficient

2.2.1. **Loss spectroscopy**

According to the Lambert-Beer law the transmitted intensity through a sample declines exponentially with increasing length L

$$I(L) = I(0)\exp(-\alpha L). \tag{8}$$

$I(0)$ is the intensity of the incident light and α the absorption coefficient of the investigated liquid per unit length. To measure the absorption coefficient as a function of the wavelength, the difference in the losses of two identically prepared samples of different lengths has to be determined [17]. For the ratio of the transmitted intensities for two liquid filled tubes of lengths L_1 and L_2 at the wavelength λ one obtains [17]

$$\frac{I_{\text{liq}}(L_1,\lambda)}{I_{\text{empty}}(L_1,\lambda)}\frac{I_{\text{empty}}(L_2,\lambda)}{I_{\text{liq}}(L_2,\lambda)} = \exp(\alpha(L_2 - L_1)). \tag{9}$$

#170502 - $15.00 USD Received 12 Jun 2012; revised 26 Sep 2012; accepted 2 Oct 2012; published 15 Oct 2012

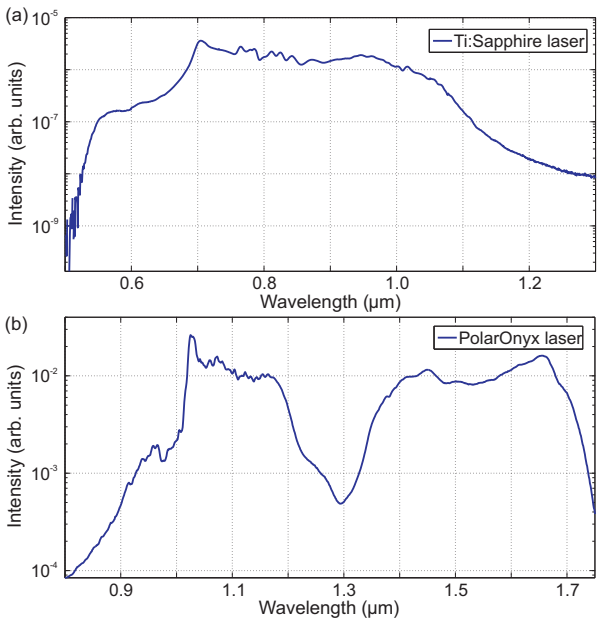

Fig. 6. White light spectra of (a) a Ti:Sapphire laser with a 2.5 μm thick tapered fiber and (b) a PolarOnyx laser with a 3.0 μm thick tapered fiber with 80 mm waist length.

As a reference signal the corresponding transmitted intensity through the empty tube I_{empty} is used. Rewriting the Eq. (9) one can calculate the absorption coefficient

$$\alpha(\lambda) = \frac{\ln\left(\frac{I_{\mathrm{liq}}(L_1,\lambda)}{I_{\mathrm{liq}}(L_2,\lambda)}\frac{I_{\mathrm{empty}}(L_2,\lambda)}{I_{\mathrm{empty}}(L_1,\lambda)}\right)}{L_2 - L_1}. \tag{10}$$

The effect of reflections at the end faces of the sample which also diminish the transmitted intensity cancels out by division of the measured intensities since for identically prepared samples these losses are the same and do not depend on the length of the tube. Furthermore, one can neglect multiple interferences according to the paper of K. C. Kao et al. [17].

2.2.2. **Absorption setup**

The experimental setup is shown in Fig. 7a. A Yokogawa AQ4305 white light source is used as light source. Because of its broad wavelength range spanning from 400 nm to 1800 nm and its very stable intensity spectrum, the light source is particularly suitable for the application of wavelength dependent loss spectroscopy.

A 4x objective with a numerical aperture of 0.10 provides a suitable collimation of the beam. The liquids are either filled into glass cells of Hellma Analytics or into quadratic stainless steel tubes with 1 mm thick microscope slides from Menzel Gläser at their end faces, depending on the absorption magnitude (see Fig. 7b). The glass cells provide shorter, the tubes longer sample lengths. The glass cell lengths vary between 1 mm and 40 mm and the tube lengths between 25 mm and 1000 mm. The collimated beam of about 7 mm diameter travels through the tubes or glass cells whose parallel end faces have to be precisely aligned perpendicular to the incoming light to avoid beam displacement. Furthermore, it has to be considered that the samples with and without the liquid are placed identically so that the reflection coefficients, which are dependent on the incident angle, remain unchanged. A system of mirrors and a lens focus the beam directly

#170502 - $15.00 USD Received 12 Jun 2012; revised 26 Sep 2012; accepted 2 Oct 2012; published 15 Oct 2012

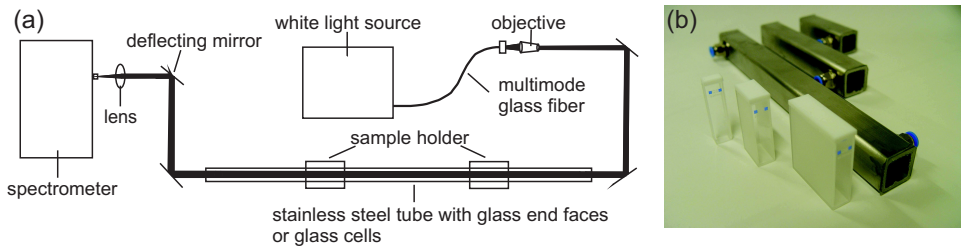

Fig. 7. (a) Experimental setup for absorption measurements in the visible and near-infrared. (b) Glass cells and stainless steel tubes enclosed with glass plates.

into the Ando AQ-6315E spectrometer with a spectral measuring range from 350 nm up to 1750 nm. With the last two mirrors one can compensate slight beam displacements to obtain a maximum detection signal.

3. Experimental data and numerical dispersion results

3.1. *Refractive indices*

At each wavelength several measurements at a temperature of 20 °C are taken to calculate the arithmetic average of $n'_{liq}(\lambda)$. With this averaged value the actual refractive index of the liquid n_{liq} is then obtained by using Eq. (6) and Eq. (7) with $n_{pr}(\lambda_D) = 1.74054$ and $\phi = 63\,°$. To calculate the uncertainties associated with the measurement, error propagation is used to account for the uncertainties in the dispersion of the prism Δn_{pr} and in the measured refractive index $\Delta n'_{liq}$. The error for the dispersion of the prism can be obtained from the standard error of the Cauchy formula (Eq. (7)) and is 1×10^{-4}. The uncertainty in n'_{liq} is given by the standard error of the single measurements. Hence, the absolute maximum error at each wavelength can be calculated by

$$\Delta n_{liq} = \left|\frac{\partial n_{liq}}{\partial n_{pr}}\right| \Delta n_{pr} + \left|\frac{\partial n_{liq}}{\partial n'_{liq}}\right| \Delta n'_{liq}. \tag{11}$$

The corrected refractive indices with their uncertainties are listed in Table 1 and Table 2 for the eight investigated liquids. The absolute maximum error $\Delta n_{liq}(\lambda)$ ranges between 1×10^{-4} and 6×10^{-4} and arise from temperature variations, reading and adjustment errors of the refractometer, the bandwidth of the filters, and errors in the dispersion of the prism. During the measuring procedure filters in 50 nm steps in the wavelength region between 500 nm and 900 nm and in 100 nm steps from 900 nm up to 1600 nm are used. Furthermore, the measurement series from the different white light sources match very well so that they can be combined and used for a single dispersion formula that covers the whole spectral range in the visible and near-infrared.

From the various refractive indices at different wavelengths one can calculate a dispersion equation by nonlinear curve fitting using the least square method. Among the various dispersion equations the Sellmeier and the Cauchy formula are the most common. The ansatz of Sellmeier can be used in the whole spectral region and is up to the second order given by

$$n^2(\lambda) = 1 + \frac{A_1\lambda^2}{\lambda^2 - B_1} + \frac{A_2\lambda^2}{\lambda^2 - B_2}, \tag{12}$$

with $A_{1/2}$ being material parameters and $\sqrt{B_{1/2}}$ the wavelengths of corresponding absorption bands.

#170502 - $15.00 USD Received 12 Jun 2012; revised 26 Sep 2012; accepted 2 Oct 2012; published 15 Oct 2012

Table 1. Experimental values of the refractive index of distilled water, heavy water, ethanol, and toluene at a temperature of 20 °C.

λ (μm)	n_{water}	$n_{\text{heavy water}}$	n_{ethanol}	n_{toluene}
0.50	1.3372 ± 0.0002	1.3315 ± 0.0002	1.3653 ± 0.0004	1.5059 ± 0.0002
0.55	1.3345 ± 0.0002	1.3294 ± 0.0002	1.3625 ± 0.0002	1.4998 ± 0.0003
0.60	1.3328 ± 0.0002	1.3278 ± 0.0002	1.3612 ± 0.0003	1.4958 ± 0.0003
0.65	1.3314 ± 0.0003	1.3264 ± 0.0002	1.3596 ± 0.0002	1.4926 ± 0.0003
0.70	1.3301 ± 0.0002	1.3258 ± 0.0002	1.3589 ± 0.0003	1.4901 ± 0.0003
0.75	1.3291 ± 0.0003	1.3248 ± 0.0002	1.3579 ± 0.0003	1.4879 ± 0.0003
0.80	1.3282 ± 0.0001	1.3240 ± 0.0002	1.3573 ± 0.0003	1.4865 ± 0.0002
0.85	1.3273 ± 0.0002	1.3235 ± 0.0002	1.3569 ± 0.0003	-
0.90	1.3263 ± 0.0003	1.3228 ± 0.0002	1.3565 ± 0.0003	1.4837 ± 0.0003
1.00	1.3249 ± 0.0002	1.3217 ± 0.0004	1.3551 ± 0.0004	1.4823 ± 0.0003
1.10	1.3235 ± 0.0003	1.3209 ± 0.0004	1.3542 ± 0.0003	1.4809 ± 0.0003
1.20	1.3218 ± 0.0004	1.3198 ± 0.0003	1.3539 ± 0.0003	1.4800 ± 0.0003
1.30	1.3201 ± 0.0002	1.3191 ± 0.0002	1.3532 ± 0.0003	1.4792 ± 0.0003
1.40	1.3183 ± 0.0003	1.3183 ± 0.0003	1.3528 ± 0.0003	1.4783 ± 0.0003
1.50	1.3167 ± 0.0004	1.3173 ± 0.0004	1.3522 ± 0.0003	1.4779 ± 0.0003
1.60	1.3141 ± 0.0004	1.3167 ± 0.0005	1.3518 ± 0.0004	1.4773 ± 0.0004

Table 2. Experimental values of the refractive index of carbon disulfide, carbon tetrachloride, chloroform, and nitrobenzene at a temperature of 20 °C.

λ (μm)	$n_{\text{carbon disulfide}}$	$n_{\text{carbon tetrachloride}}$	$n_{\text{chloroform}}$	$n_{\text{nitrobenzene}}$
0.50	1.6473 ± 0.0003	1.4652 ± 0.0002	1.4495 ± 0.0003	1.5671 ± 0.0002
0.55	1.6348 ± 0.0006	1.4616 ± 0.0002	1.4461 ± 0.0002	1.5574 ± 0.0003
0.60	1.6266 ± 0.0004	1.4595 ± 0.0002	1.4434 ± 0.0002	1.5505 ± 0.0005
0.65	1.6186 ± 0.0005	1.4570 ± 0.0003	1.4418 ± 0.0002	1.5456 ± 0.0003
0.70	1.6136 ± 0.0005	1.4558 ± 0.0002	1.4402 ± 0.0004	1.5420 ± 0.0003
0.75	1.6091 ± 0.0003	1.4547 ± 0.0002	1.4391 ± 0.0002	1.5390 ± 0.0002
0.80	1.6058 ± 0.0004	1.4536 ± 0.0002	1.4383 ± 0.0003	1.5367 ± 0.0004
0.85	1.6032 ± 0.0005	1.4523 ± 0.0002	1.4374 ± 0.0003	1.5346 ± 0.0004
0.90	1.6008 ± 0.0005	1.4519 ± 0.0002	1.4369 ± 0.0005	1.5333 ± 0.0002
1.00	1.5976 ± 0.0004	1.4512 ± 0.0003	1.4357 ± 0.0004	1.5307 ± 0.0003
1.10	1.5947 ± 0.0004	1.4504 ± 0.0003	1.4351 ± 0.0004	1.5290 ± 0.0003
1.20	1.5929 ± 0.0003	1.4497 ± 0.0004	1.4346 ± 0.0003	1.5273 ± 0.0002
1.30	1.5909 ± 0.0005	1.4491 ± 0.0004	1.4342 ± 0.0003	1.5264 ± 0.0003
1.40	1.5900 ± 0.0004	1.4488 ± 0.0004	1.4340 ± 0.0003	1.5256 ± 0.0003
1.50	1.5888 ± 0.0003	1.4484 ± 0.0003	1.4335 ± 0.0003	1.5247 ± 0.0003
1.60	1.5880 ± 0.0004	1.4479 ± 0.0003	1.4332 ± 0.0003	1.5240 ± 0.0003

Far away from any resonance one can use the simpler Cauchy equation. Therefore the first order Sellmeier equation can be expanded into a power series. Up to the second order one obtains

$$n^2(\lambda) = 1 + \frac{A_1\lambda^2}{\lambda^2 - B_1} \approx 1 + A_1\left(1 + \frac{B_1}{\lambda^2} + \frac{B_1^2}{\lambda^4}\right) = C_0 + \frac{C_1}{\lambda^2} + \frac{C_2}{\lambda^4}. \tag{13}$$

An improvement in fitting the refractive index of liquids in the visible to near-infrared region can be expected if a term $C_3\lambda^2$ in Eq. (13) is added due to infrared vibrational absorption

#170502 - $15.00 USD Received 12 Jun 2012; revised 26 Sep 2012; accepted 2 Oct 2012; published 15 Oct 2012

bands [15] which leads to

$$n^2(\lambda) = C_0 + \frac{C_1}{\lambda^2} + \frac{C_2}{\lambda^4} + C_3\lambda^2. \tag{14}$$

For each liquid the constants of the Sellmeier and the Cauchy formulas are calculated. To choose the number of terms, the standard error of the constants, the summed squares of residuals (SSE), the adjusted R-square, and the fit standard error (Root Mean Squared Error, RMSE) are taken into account.

By careful comparison of the fitting results it turns out that one or two terms in the Sellmeier formula (Eq. (12)) deliver satisfying results. However, the additional term in Eq. (14) offers indeed better fitting results than Eq. (13) for the Cauchy formula.

In Table 3 and Table 4 the constants of Sellmeier and Cauchy formula and their statistics are given for each liquid. The values of the standard deviation indicate good quality of the fits. The error for n^2_{liq} is in the best case about 3.0×10^{-4} for chloroform and still below 6.2×10^{-4} for carbon tetrachloride in the worst case.

Sellmeier and Cauchy formulas shown in the following Figs. 8, 9, 10, 11, 12, 13, 14, 15 are based on data between wavelengths of 500 nm and 1600 nm. For reasons of clarity no absolute error bars associated with each measured refractive index value are plotted. In general, the refractive index in the wavelength range of the visible to the near-infrared is caused by electronic absorption in the ultraviolet and the vibrational absorption in the infrared. In the following previously published data are shown in comparison, being in very good agreement with our measurements.

3.1.1. **Refractive index of distilled water**

In Fig. 8 the measured values for the refractive index of distilled water are shown which are listed in Table 1. We plotted there as well the Sellmeier formula given in Table 3 together with reference values from Refs. [16, 18, 21]. For distilled water many reference data have been published; only three are shown in Fig. 8. The dispersion curve from Ref. [18] is plotted in the wavelength range between 405 nm and 1129 nm. From a wavelength of 800 nm upwards the

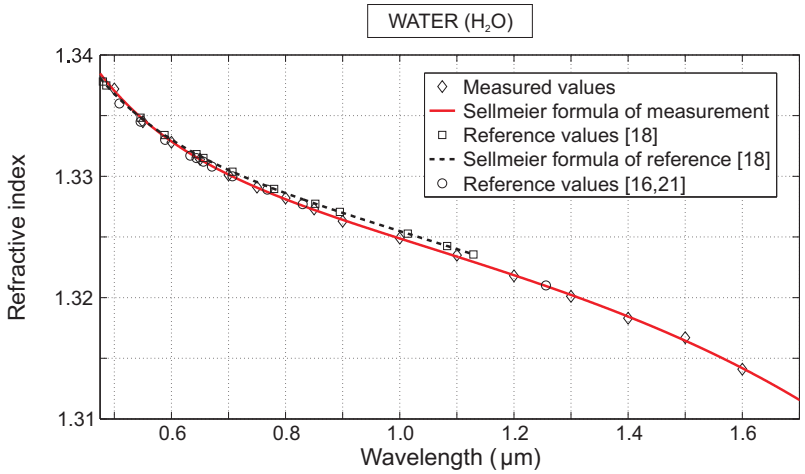

Fig. 8. Dispersion of the linear refractive index of liquid water at a temperature of 20 °C. Diamonds represent the experimental data listed in Table 1; the solid red curve is the calculated Sellmeier dispersion formula given in Table 3; for comparison we also plotted the reference data as squares and the corresponding dispersion curve (dashed black line) from Ref. [18]. Circles are published data extracted from Refs. [16, 21].

#170502 - $15.00 USD Received 12 Jun 2012; revised 26 Sep 2012; accepted 2 Oct 2012; published 15 Oct 2012

Table 3. Constants of Sellmeier and Cauchy formula of distilled water, heavy water, chloroform, and carbon tetrachloride at a temperature of 20 °C.

Parameter	Sellmeier formula $y = n^2(A_1, B_1, A_2, B_2)$	Parameter	Cauchy formula $y = n^2(C_0, C_1, C_2, C_3)$
WATER			
A_1	0.75831 ± 0.00082	C_0	1.76880 ± 0.00134
B_1 (μm^{-2})	0.01007 ± 0.00027	C_1 (μm^2)	0.00237 ± 0.00093
A_2	0.08495 ± 0.01912	C_2 (μm^4)	0.00087 ± 0.00017
B_2 (μm^{-2})	8.91377 ± 1.35076	C_3 (μm^{-2})	-0.01651 ± 0.00048
SSE (10^{-6})	1.57	SSE (10^{-6})	1.92
Adj. R-Square	0.99957	Adj. R-Square	0.99948
RMSE (10^{-4})	3.62	RMSE (10^{-4})	4.00
HEAVY WATER			
A_1	-0.30637 ± 0.76766	C_0	1.74679 ± 0.00108
B_1 (μm^{-2})	-47.26686 ± 126.47658	C_1 (μm^2)	0.00633 ± 0.00075
A_2	0.74659 ± 0.00104	C_2 (μm^4)	0.00014 ± 0.00014
B_2 (μm^{-2})	0.00893 ± 0.00031	C_3 (μm^{-2})	-0.00623 ± 0.00038
SSE (10^{-6})	1.26	SSE (10^{-6})	1.24
Adj. R-Square	0.99922	Adj. R-Square	0.99922
RMSE (10^{-4})	3.24	RMSE (10^{-4})	3.22
CHLOROFORM			
A_1	1.04647 ± 0.00921	C_0	2.05159 ± 0.00100
B_1 (μm^{-2})	0.01048 ± 0.00130	C_1 (μm^2)	0.01005 ± 0.00069
A_2	0.00345 ± 0.00941	C_2 (μm^4)	0.00059 ± 0.00013
B_2 (μm^{-2})	0.15207 ± 0.09540	C_3 (μm^{-2})	-0.00052 ± 0.00035
SSE (10^{-6})	1.13	SSE (10^{-6})	1.06
Adj. R-Square	0.99951	Adj. R-Square	0.99954
RMSE (10^{-4})	3.07	RMSE (10^{-4})	2.98
CARBON TETRACHLORIDE			
A_1	1.09215 ± 0.00027	C_0	2.09503 ± 0.00208
B_1 (μm^{-2})	0.01187 ± 0.00012	C_1 (μm^2)	0.01102 ± 0.00144
		C_2 (μm^4)	0.00050 ± 0.00026
		C_3 (μm^{-2})	-0.00102 ± 0.00074
SSE (10^{-6})	5.35	SSE (10^{-6})	4.61
Adj. R-Square	0.99826	Adj. R-Square	0.99826
RMSE (10^{-4})	6.18	RMSE (10^{-4})	6.20

#170502 - $15.00 USD Received 12 Jun 2012; revised 26 Sep 2012; accepted 2 Oct 2012; published 15 Oct 2012

Table 4. Constants of Sellmeier and Cauchy formula of toluene, ethanol, carbon disulfide, and nitrobenzene at a temperature of 20 °C.

Parameter	Sellmeier formula $y = n^2(A_1, B_1, A_2, B_2)$	Parameter	Cauchy formula $y = n^2(C_0, C_1, C_2, C_3)$
TOLUENE			
A_1	1.17477 ± 0.00022	C_0	2.17873 ± 0.00138
B_1 (μm^{-2})	0.01825 ± 0.00009	C_1 (μm^2)	0.01886 ± 0.00095
		C_2 (μm^4)	0.00086 ± 0.00017
		C_3 (μm^{-2})	-0.00145 ± 0.00049
SSE (10^{-6})	3.20	SSE (10^{-6})	1.82
Adj. R-Square	0.99964	Adj. R-Square	0.99976
RMSE (10^{-4})	4.96	RMSE (10^{-4})	4.07
ETHANOL			
A_1	0.83189 ± 0.00196	C_0	1.83347 ± 0.00199
B_1 (μm^{-2})	0.00930 ± 0.00052	C_1 (μm^2)	0.00648 ± 0.00138
A_2	-0.15582 ± 1.59085	C_2 (μm^4)	0.00031 ± 0.00025
B_2 (μm^{-2})	-49.45200 ± 537.47222	C_3 (μm^{-2})	-0.00352 ± 0.00071
SSE (10^{-6})	4.53	SSE (10^{-6})	4.23
Adj. R-Square	0.99667	Adj. R-Square	0.99689
RMSE (10^{-4})	6.15	RMSE (10^{-4})	5.94
CARBON DISULFIDE			
A_1	1.50387 ± 0.00027	C_0	2.50984 ± 0.00161
B_1 (μm^{-2})	0.03049 ± 0.00008	C_1 (μm^2)	0.04101 ± 0.00112
		C_2 (μm^4)	0.00252 ± 0.00021
		C_3 (μm^{-2})	-0.00183 ± 0.00057
SSE (10^{-6})	5.84	SSE (10^{-6})	2.77
Adj. R-Square	0.99987	Adj. R-Square	0.99993
RMSE (10^{-4})	6.46	RMSE (10^{-4})	4.81
NITROBENZENE			
A_1	1.30628 ± 0.00449	C_0	2.31952 ± 0.00125
B_1 (μm^{-2})	0.02268 ± 0.00079	C_1 (μm^2)	0.02355 ± 0.00087
A_2	0.00502 ± 0.00474	C_2 (μm^4)	0.00266 ± 0.00016
B_2 (μm^{-2})	0.18487 ± 0.02830	C_3 (μm^{-2})	-0.00259 ± 0.00044
SSE (10^{-6})	2.57	SSE (10^{-6})	1.67
Adj. R-Square	0.99986	Adj. R-Square	0.99991
RMSE (10^{-4})	4.63	RMSE (10^{-4})	3.73

#170502 - $15.00 USD Received 12 Jun 2012; revised 26 Sep 2012; accepted 2 Oct 2012; published 15 Oct 2012

red solid and dashed black lines run nearly parallel to each other with a maximum deviation of 6×10^{-4}. Also, the values given in the Refs. [16] and [21] match very well with our data. Moreover, a Cauchy formula from Ref. [16] in the range between 486 nm and 943 nm and the values of Ref. [22] fit quite well our own measured values but are not shown in Fig. 8 for reasons of clarity.

In general, the trend of dispersion of water differs from that of the other investigated liquids due to the huge vibrational overtone absorption band at a wavelength of around 1400 nm (see Fig. 16).

3.1.2. **Refractive index of heavy water**

In Fig. 9 the measured values for the refractive index of heavy water are shown which are also listed in Table 1. Presented there as well are the Sellmeier data given in Table 3 together with reference values from Ref. [21]. The corresponding dispersion curve is plotted in the wavelength range between 405 nm and 768 nm. In this regime the solid red and the dashed black lines show good agreement and deviate between 1.5×10^{-4} and 4.5×10^{-4}. The deviations of the extended Cauchy formula derived in Ref. [21] from our own Sellmeier formula increase with increasing wavelength which indicates the limited usability of dispersion curves beyond their measuring range. Furthermore, we observe a weaker influence of the first overtone vibration on the dispersion curve compared to H_2O since the absorption band is shifted to higher wavelengths (around 2.1 μm). This effect results from the heavier deuterium nucleus (see Fig. 17).

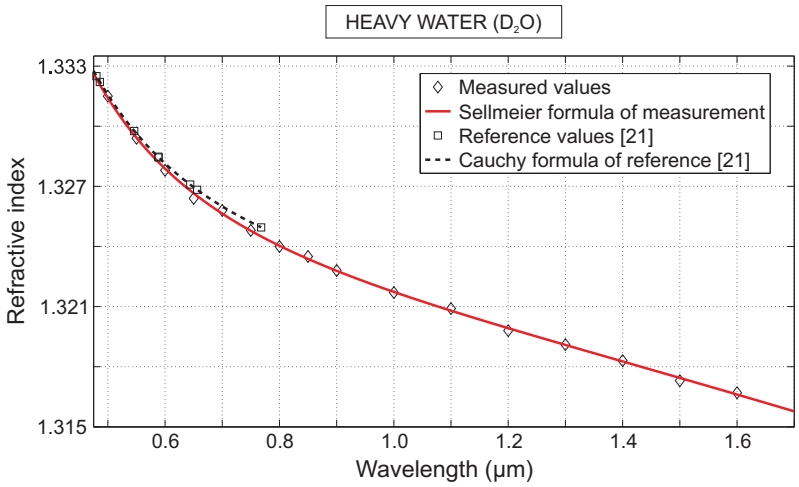

Fig. 9. Dispersion of the linear refractive index of liquid heavy water at a temperature of 20 °C. Diamonds represent the experimental data listed in Table 1; the solid red curve represents the calculated Sellmeier dispersion formula given in Table 3; for comparison we also plotted the reference data as squares and the corresponding dispersion curve (dashed black line) from Ref. [21].

3.1.3. **Refractive index of chloroform**

In Fig. 10 the measured values for the refractive index of chloroform are shown which are listed in Table 2. Presented there as well are the Sellmeier data from Table 3 together with reference values from Ref. [22]. The single data points from Ref. [22] match very good with the solid red curve and the deviations lie always below 4×10^{-4}. We observe a deviation of at

#170502 - $15.00 USD Received 12 Jun 2012; revised 26 Sep 2012; accepted 2 Oct 2012; published 15 Oct 2012

maximum 20×10^{-4} in comparison to Ref. [15]. In this reference the data points are located in the wavelength range between 265 nm and 2480 nm, however, with a lack of measured values between 656 nm and 2130 nm which is the reason for this huge deviation. Dispersion effects due to the absorption bands displayed in Fig. 18 have not been found since the vibrational overtones are too weak in the infrared range.

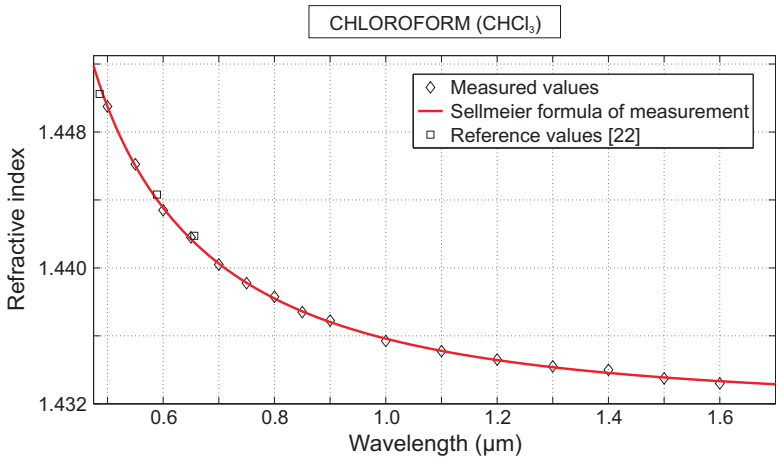

Fig. 10. Dispersion of the linear refractive index of liquid chloroform at a temperature of 20 °C. Diamonds represent the experimental data listed in Table 2; the solid red curve is the calculated Sellmeier dispersion formula given in Table 3; also shown is for comparison the reference data from Ref. [22] as squares.

3.1.4. **Refractive index of carbon tetrachloride**

In Fig. 11 the measured values for the refractive index of carbon tetrachloride are plotted as listed in Table 2. Presented as well is our Cauchy fit from Table 3 together with reference

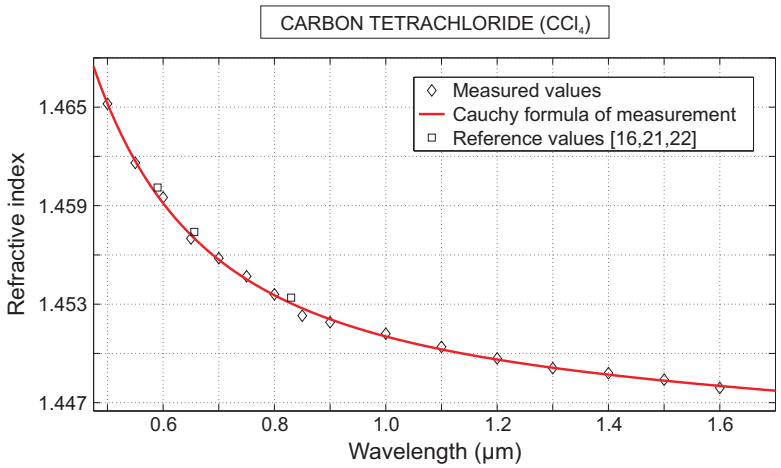

Fig. 11. Dispersion of the linear refractive index of liquid carbon tetrachloride at a temperature of 20 °C. Diamonds represent the experimental data listed in Table 2; the solid red curve is the calculated Cauchy dispersion formula given in Table 3; for comparison we show the reference data from Refs. [16, 21, 22] as squares.

#170502 - $15.00 USD Received 12 Jun 2012; revised 26 Sep 2012; accepted 2 Oct 2012; published 15 Oct 2012

values from Refs. [16, 21, 22]. The three single reference data points lie slightly above the red solid curve, but differ not more than 4×10^{-4}. Due to the consistently small absorption coefficient (see Fig. 19) no influences on the dispersion trend are noticeable.

3.1.5. **Refractive index of toluene**

In Fig. 12 we plot the measured values for the refractive index of toluene which are listed in Table 1. Presented there as well are the Cauchy data given in Table 4 together with reference values from Refs. [16, 22]. The dispersion curve from Ref. [15] is plotted in the wavelength range between 405 nm and 830 nm. The solid red and dashed black curve match very well, and the largest deviation above a wavelength of 600 nm is less than 2×10^{-4}. Also the measured reference value of Ref. [16] derived with the Abbe refractometer at a wavelength of $\lambda = 830$ nm differs less than 1×10^{-4}. The steep decline of the refractive index of toluene is not affected by the observed resonances shown in Fig. 20.

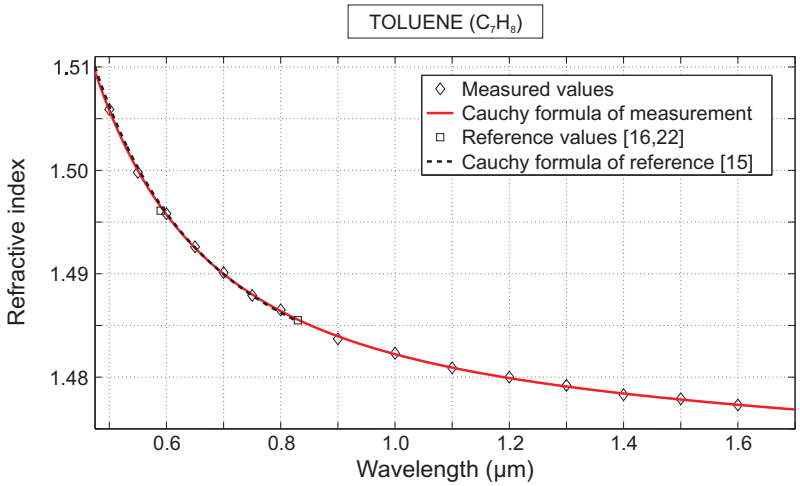

Fig. 12. Dispersion of the linear refractive index of liquid toluene at a temperature of 20 °C. Diamonds represent the experimental data listed in Table 1; the solid red curve is the calculated Cauchy dispersion formula given in Table 4; for comparison we also plotted the reference data from Refs. [16, 22] as squares as well as the dispersion curve (dashed black line) from Ref. [15].

3.1.6. **Refractive index of ethanol**

In Fig. 13 the measured values for the refractive index of ethanol are shown as given in Table 1. Presented there are also the Sellmeier data given in Table 4 together with reference values from Refs. [16, 21, 22]. The dispersion curve from Ref. [16] is plotted in the wavelength range between 476 nm and 633 nm. The solid red and dashed black curve agree very well and do not differ more than 2×10^{-4}. The reference data point from Ref. [16] at a wavelength of $\lambda = 830$ nm varies not more than 1×10^{-4} from our own Sellmeier equation, whereas the other points from Refs. [21,22] a more scattered. The bend of the solid red curve is slightly influenced by the strong absorption bands at a wavelength of around 1500 nm shown in Fig. 21.

#170502 - $15.00 USD Received 12 Jun 2012; revised 26 Sep 2012; accepted 2 Oct 2012; published 15 Oct 2012

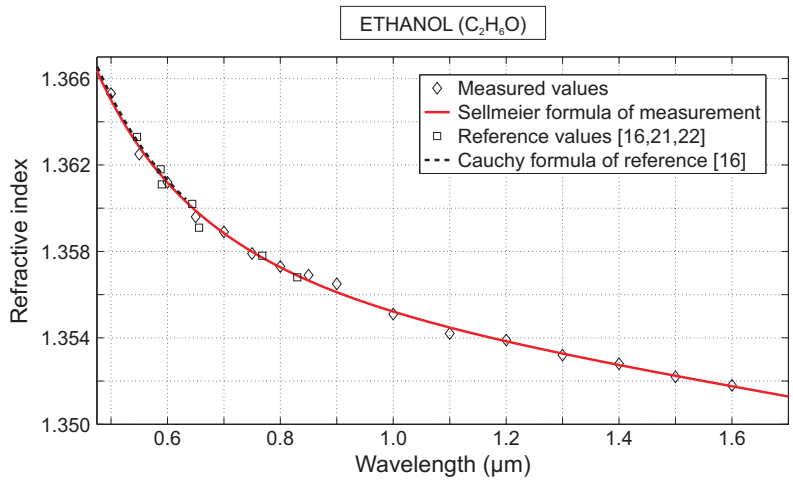

Fig. 13. Dispersion of the linear refractive index of liquid ethanol at a temperature of 20 °C. Diamonds represent the experimental data listed in Table 1; the solid red curve is the calculated Sellmeier dispersion formula given in Table 4; for comparison we also plotted the reference data as squares from Refs. [16, 21, 22] and the dispersion curve (dashed black line) from Ref. [16].

3.1.7. **Refractive index of carbon disulfide**

In Fig. 14 the measured values for the refractive index of carbon disulfide are displayed as listed in Table 2. We also plot the Cauchy fit as given in Table 4 together with the dispersion curve from Ref. [15] plotted in the wavelength range between 340 nm and 2430 nm. The trend of the solid red and dashed black curve match very well. Due to the very steep decline of the refractive index the maximal deviation is around 8×10^{-4}.

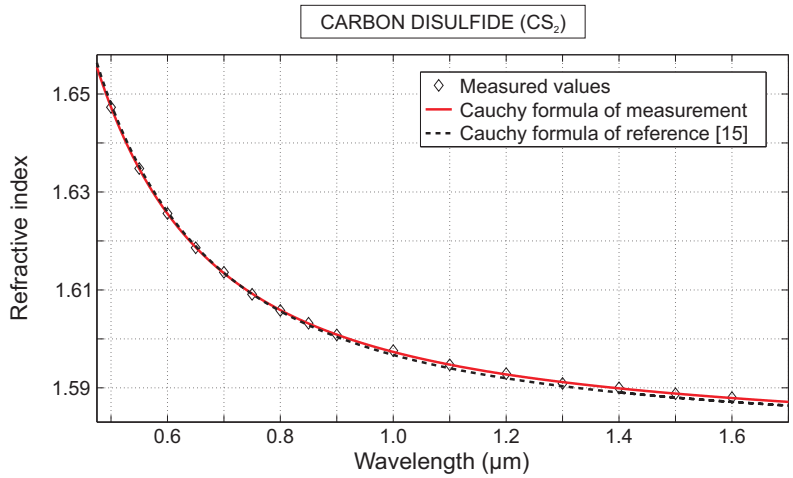

Fig. 14. Dispersion of the linear refractive index of liquid carbon disulfide at a temperature of 20 °C. Diamonds represent the experimental data listed in Table 2; the solid red curve is the calculated Cauchy dispersion formula given in Table 4; for comparison we also plotted the dispersion curve (dashed black line) from Ref. [15].

#170502 - $15.00 USD Received 12 Jun 2012; revised 26 Sep 2012; accepted 2 Oct 2012; published 15 Oct 2012

3.1.8. **Refractive index of nitrobenzene**

In Fig. 15 the measured values for the refractive index of nitrobenzene are shown which are listed in Table 2. Presented there as well is the Cauchy formula given in Table 4 together with reference values from Ref. [22]. The difference between the solid red curve and the reference data points lies between 7×10^{-4} and 9×10^{-4}. There also exist published data in Ref. [21] which differ between 4×10^{-4} and 26×10^{-4} from our own Cauchy equation. The considerable variations in the deviations result from the multitude of different reference sources mentioned in the Handbook of Nikogosyan [21].

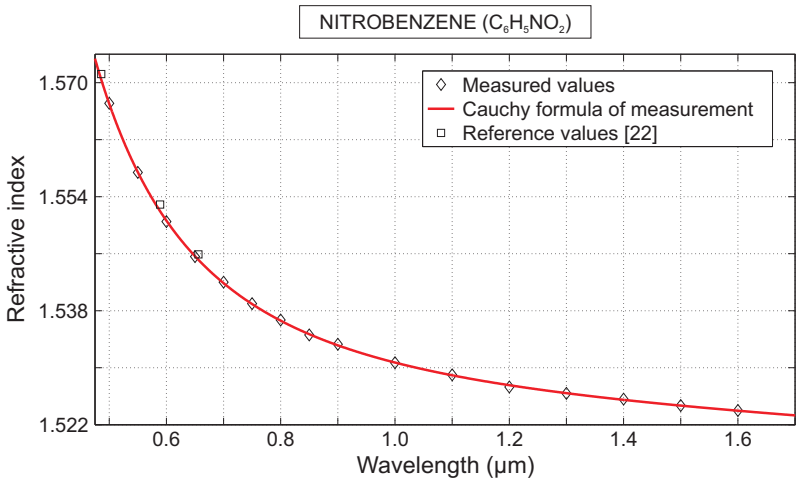

Fig. 15. Dispersion of the linear refractive index of liquid nitrobenzene at a temperature of 20 °C. Diamonds represent the experimental data listed in Table 2; the solid red curve is the calculated Cauchy dispersion formula given in Table 4; for comparison we also plotted the reference data from Ref. [22] as squares.

3.2. Absorption coefficients

At each tube length several measurements at a room temperature of 20 °C are taken to minimize the effect of unequal coupling into the spectrometer. From the transmission spectra for each tube length with and without liquid filling one can calculate the wavelength dependent absorption coefficient by Eq. (10). An average absorption coefficient can be calculated from several possible combinations of the different sample lengths. On the one hand, at wavelengths with strong absorption, only the short glass cells provide meaningful results because they can best follow the steep rise and decline at the resonance positions. More light can be collected by the spectrometer with the short cells. On the other hand at weak absorption regimes the long tube lengths deliver more precise results since they can resolve the reduced effect of the absorption by an increased propagation length (see Eq. (8)). All values of the absorption coefficient of the six investigated liquids and their standard error are given in the appendix as comma-separated value text files. The uncertainty at each wavelength is calculated by the standard deviation of the average value. Generally, the absolute standard error is quite small, but for low values of the absorption coefficient the relative deviation can become large as can also be seen in the comparison with reference values in the water measurement in Section 3.2.1.

#170502 - $15.00 USD Received 12 Jun 2012; revised 26 Sep 2012; accepted 2 Oct 2012; published 15 Oct 2012

3.2.1. **Absorption of distilled water**

In Fig. 16 the measured absorption coefficient of distilled water together with the reference values of Ref. [22] are shown. The trend of the solid red and dashed black curve match well apart from the height of the resonance peak at a wavelength of around 1450 nm. In Ref. [19] an absorption coefficient of about 24 cm^{-1} at the 1450 nm resonance peak is given. The deviation of the peak heights at resonance positions can be related to the limited response and sensitivity of the spectrometer. In our measurements cells not thinner than 1 mm and 2 mm are available to increase the transmitted intensities.

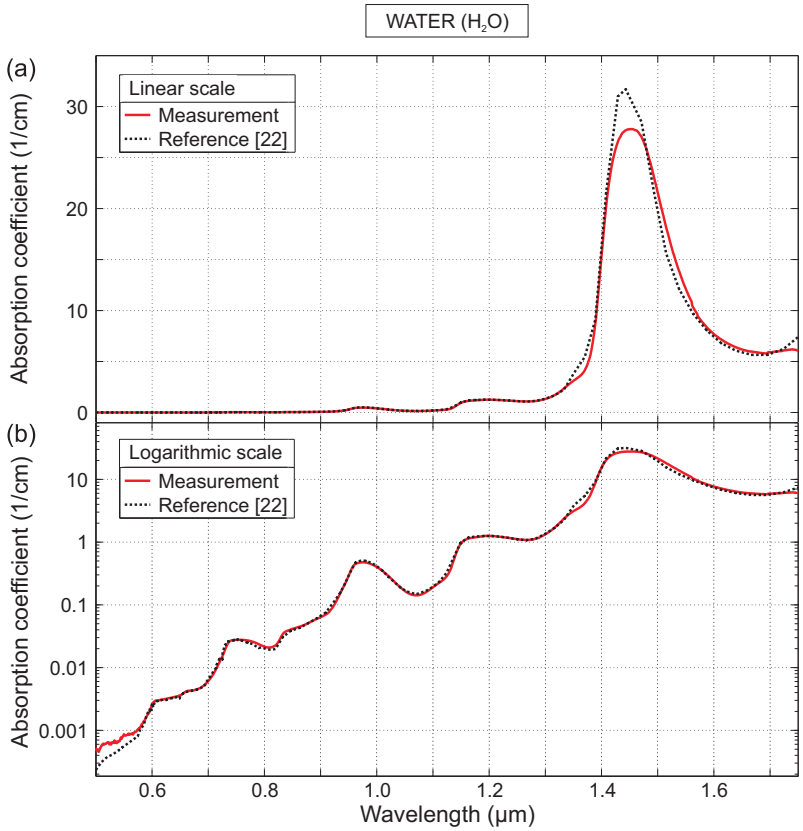

Fig. 16. Measured absorption coefficient of liquid distilled water at a temperature of 20 °C on (a) linear and (b) logarithmic scale as a function of wavelength. For comparison to our measured values (solid red line) we also plotted linearised reference data (dashed black line) from Ref. [22] (Media 1).

A first larger absorption band occurs at a wavelength of 980 nm followed by another band at around 1200 nm. The huge absorption band at a wavelength of around 1450 nm results from the first overtone stretch vibration of the water molecule. The other two bands result from higher overtones or combination vibrations. Our own measured resonance positions fit excellent to the resonances mentioned in Ref. [19].

Upon comparison with the values of Refs. [19, 22], the used measurement method can be successfully verified. Above a wavelength of 600 nm the relative deviation between the solid red and dashed black curve is at its maximum 17 % but mostly clearly below except at the steep rise at the wavelength of around 1365 nm where the difference is around 26 %. In the

#170502 - $15.00 USD Received 12 Jun 2012; revised 26 Sep 2012; accepted 2 Oct 2012; published 15 Oct 2012

range between 500 nm to 600 nm in which the absorption coefficient falls below $1 \times 10^{-3}\,\mathrm{cm}^{-1}$, the relative deviation can become large. However, the average relative deviation over the full measurement range is only 8.5 %.

Possible error sources arise from the different incoupling into the spectrometer entrance, the temporal instability of the white light source, dust on the end faces or in the liquid, temperature variations, the measurement inaccuracy of the spectrometer, and slightly different reflection coefficients at the interfaces. The main error from the slight difference in beam incoupling can be minimized by several measurements searching each time for the highest detection signal by fine adjustments of the mirrors. All together, these errors can serve as explanation for the standard deviation as well as for the differences between our measurements and the references for distilled water. However, these effects will cause uncertainties in further measurements and have to be minimized.

3.2.2. **Absorption of heavy water**

In Fig. 17 the measured absorption coefficient of heavy water is shown. In contrast to H_2O the absorption bands are considerably weaker and shifted to higher wavelengths due to the heavier deuterium nucleus. Resonance positions occur at a wavelength of around 1000 nm, 1330 nm, and 1600 nm. Because only the shorter glass cells are applied for measuring the absorption coefficient below a wavelength of 1200 nm, the measurement is noisy. Some reference data

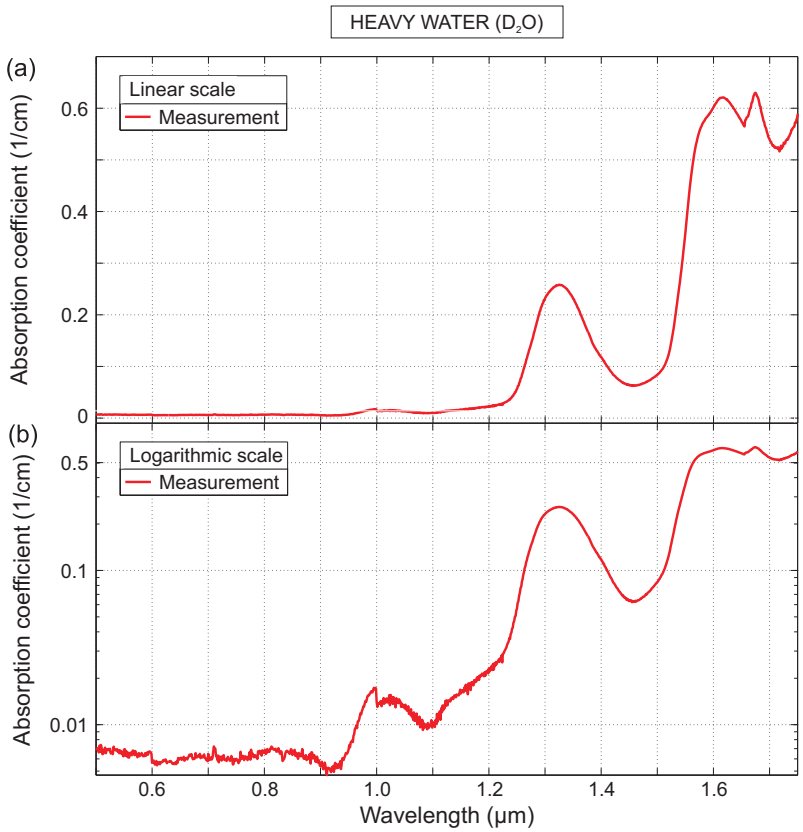

Fig. 17. Measured absorption coefficient of liquid heavy water at a temperature of 20 °C on (a) linear and (b) logarithmic scale as a function of wavelength (Media 2).

#170502 - $15.00 USD Received 12 Jun 2012; revised 26 Sep 2012; accepted 2 Oct 2012; published 15 Oct 2012

have been published in Ref. [22] for the wavelength range between 400 nm and 790 nm. In this reference the values for the absorption coefficient are clearly smaller and lie between $0.3 \times 10^{-3}\,\mathrm{cm}^{-1}$ and $1.0 \times 10^{-3}\,\mathrm{cm}^{-1}$. The deviation results from the application of the shorter glass cells instead of the longer tubes in this wavelength region with very low absorption. We did not use the longer tubes for the absorption measurement in the visible due to the high cost of heavy water.

3.2.3. **Absorption of chloroform**

In Fig. 18 the measured absorption coefficient of chloroform is shown. The absorption bands of chloroform are relatively narrow when compared with water. They arise from overtones of the CH-group stretch mode and from combination vibrations. Additionally to the sharp peaks at a wavelength of around 1150 nm, 1420 nm, and 1680 nm, numerous smaller peaks below an absorption coefficient of $0.2\,\mathrm{cm}^{-1}$ can be observed. The large peak at a wavelength of 1680 nm could only be measured exactly when using the thinnest glass cells of 1 mm and 2 mm length, whereas the smaller peaks are only visible with the longest tubes.

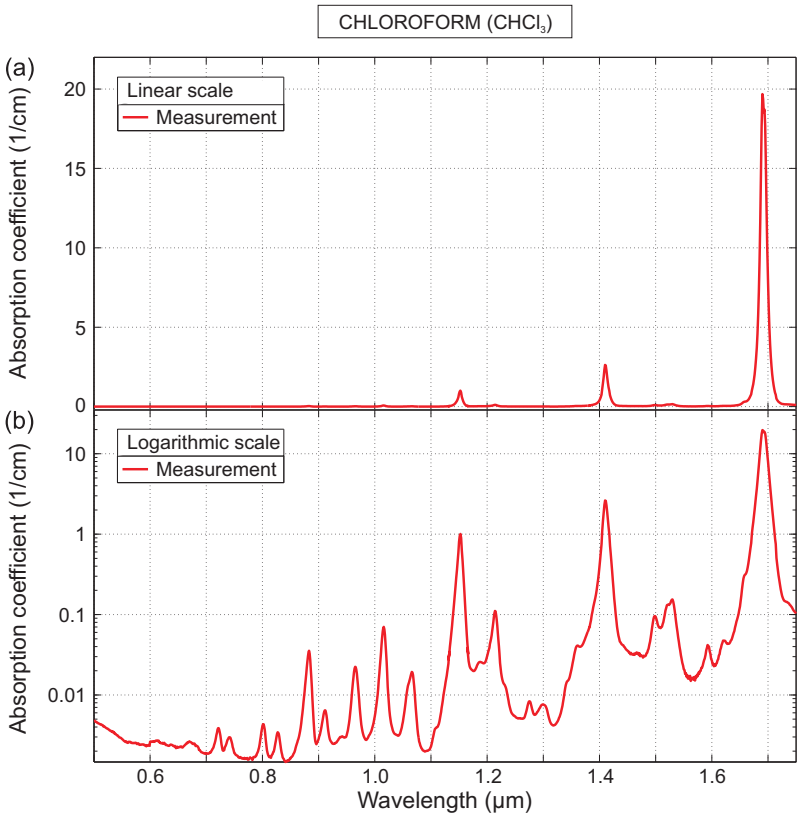

Fig. 18. Measured absorption coefficient of liquid chloroform at a temperature of 20 °C on (a) linear and (b) logarithmic scale as a function of wavelength (Media 3).

3.2.4. **Absorption of carbon tetrachloride**

In Fig. 19 the measured absorption coefficient of carbon tetrachloride is shown. Due to the consistently small absorption coefficient α, which never exceeds $6 \times 10^{-3}\,\mathrm{cm}^{-1}$, only the longest

#170502 - $15.00 USD Received 12 Jun 2012; revised 26 Sep 2012; accepted 2 Oct 2012; published 15 Oct 2012

tubes of 250 mm, 500 mm, 750 mm, and 1000 mm length are used to determine the value of α. The wavelength range only spans from 500 nm up to 1500 nm as the glass cell measurements above 1500 nm are dominated by noise.

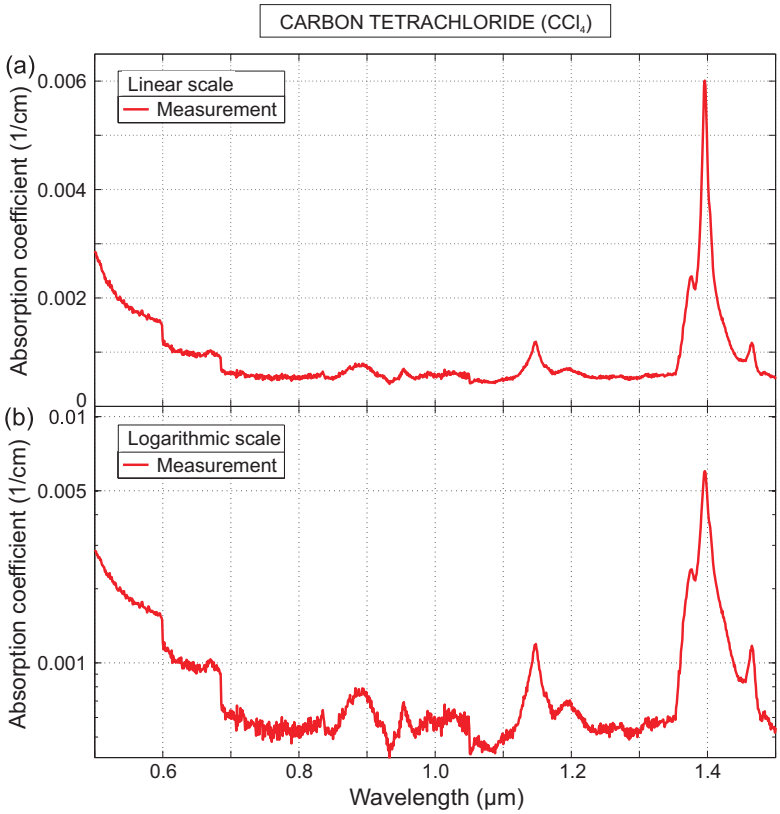

Fig. 19. Measured absorption coefficient of liquid carbon tetrachloride at a temperature of 20 °C on (a) linear and (b) logarithmic scale as a function of wavelength (Media 4).

3.2.5. **Absorption of toluene**

In Fig. 20 the measured absorption coefficient of toluene is shown. The same shapes of the three absorption bands at a wavelength of around 730 nm, 900 nm, and 1150 nm with decreasing intensities indicate higher vibrational overtones. The pronounced peak at a wavelength of around 1700 nm could not be fully resolved due to the decreasing intensity of the white light source at this wavelength range. Toluene consists of a benzene ring with an additional CH_3-group. Amongst others, the absorption bands result from stretching overtones of the CH- and CH_3-group.

3.2.6. **Absorption of ethanol**

In Fig. 21 the measured absorption coefficient of ethanol is shown. The spectra are dominated by vibrational overtones from the groups CH_2, CH_3 and CH_2OH. The shapes of the absorption bands at wavelengths of around 630 nm, 730 nm, 930 nm, and 1200 nm are very similar. Also the peak at a wavelength of around 1700 nm could be not fully assessed.

#170502 - $15.00 USD Received 12 Jun 2012; revised 26 Sep 2012; accepted 2 Oct 2012; published 15 Oct 2012

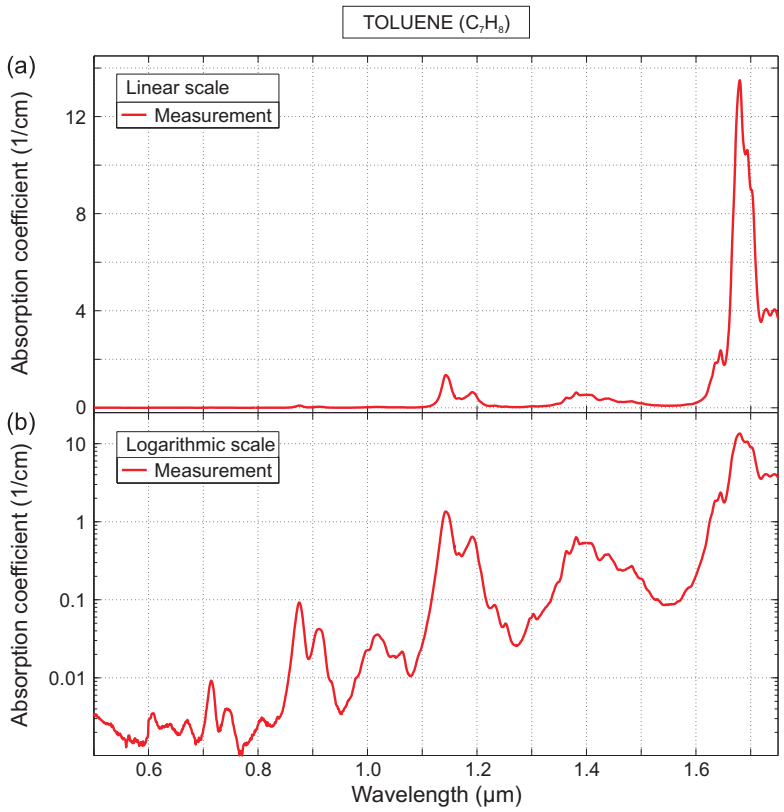

Fig. 20. Measured absorption coefficient of liquid toluene at a temperature of 20 °C on (a) linear and (b) logarithmic scale as a function of wavelength (Media 5).

4. Conclusion

The dispersion and absorption properties of several frequently used nonlinear liquids in the visible and near-infrared have been measured at a temperature of 20 °C. The refractive index measurement requires the calculation of correction terms in order to use a standard Abbe refractometer in a wider wavelength region beyond the visible. Comparisons with original corrections from Zeiss confirm the used method. All modifications which are needed to extend the application range are described and given in detail. Accurate measurement data between a wavelength range from 500 nm up to 1600 nm together with their fitting constants of Cauchy and Sellmeier equations are given for the first time over this broad wavelength region and were successfully compared with sparsely existing published data.

The described technique can easily be applied and extended to longer wavelengths above 1600 nm with suitable cameras and more powerful and broadband white light sources. A limiting factor due to the transmittance of lenses, prism, and their coatings according to Ref. [16] could not be observed in our spectral range. Strongly absorbing liquids such as water or ethanol have to be investigated in reflection mode and may cause problems at higher wavelengths due to a reduction of the image contrast. Moreover, the refraction index measurement with the Abbe refractometer can be easily transferred to further liquids. An improvement in accuracy could be achieved by a more stable cooling system.

The absorption coefficient α can be determined from the transmitted intensity through cells or tubes of different lengths. Due to the fact that each value α is calculated by using two

#170502 - $15.00 USD Received 12 Jun 2012; revised 26 Sep 2012; accepted 2 Oct 2012; published 15 Oct 2012

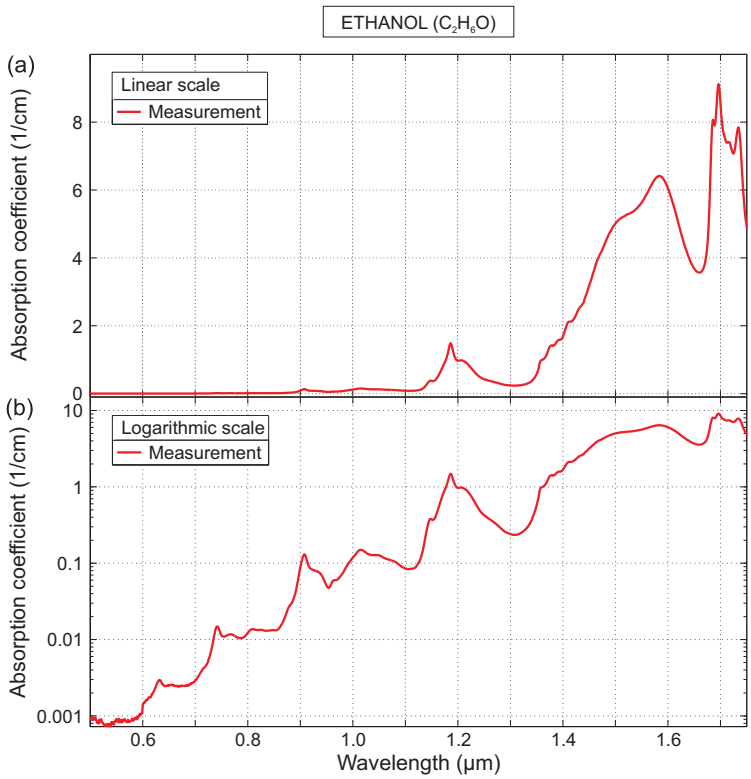

Fig. 21. Measured absorption coefficient of liquid ethanol at a temperature of 20 °C on (a) linear and (b) logarithmic scale as a function of wavelength (Media 6).

different length combinations, identical positioning and preparation of the samples have to be taken into account. Also the suitable choice of cells or tubes depending on the magnitude of absorption have to be considered. For small values of the absorption coefficient the longer tubes are ideal, whereas at absorption resonances the thinner glass cells provide meaningful results. The measurement technique could be successfully verified by comparison with reference data for distilled water. Measurements in a wavelength region between 500 nm and 1750 nm (for CCl_4 only up to a wavelength of 1500 nm) were taken.

The used technique can also easily be extended to other liquids and different wavelengths. However, for strongly absorbing liquids the application range is restricted because of the available thicknesses of the glass cells below 1 mm. The transmitted intensity could be increased by a more powerful white light laser, however possibly at the expense of spectral stability and therefore also leading to reduced accuracy.

In general, the presented methods provide an easy and accurate way to determine the refractive index and the absorption coefficient of liquids. If the desired liquid is not included in the collection presented in this paper, all necessary information are provided here to transfer these techniques and apply them to the liquid of interest.

Acknowledgments

This work was supported financially by DFG, BMBF, GIF, BW-Stiftung, and Alexander von Humboldt Stiftung. We acknowledge support from the German Research Foundation (DFG) within the funding program Open Access Publishing.

#170502 - $15.00 USD Received 12 Jun 2012; revised 26 Sep 2012; accepted 2 Oct 2012; published 15 Oct 2012